UAV-BASED MULTISPECTRAL IMAGING FOR SURFACE OIL AND WATER LEAK DETECTION OVER SOIL USING DEEP LEARNING

Dimple Bhuta[1], Anand Siyote[1], Sanket Bhegde[1], Rohit Kushwaha[1], Saptajit Banerjee[1], Hemendra Arya[2]
[1]*TIH Foundation for IoT & IoE, IIT Bombay, Mumbai, India*
[2]*Department of Aerospace Engineering, IIT Bombay, Mumbai, India*

***Abstract*—Pipeline leakages involving oil and water pose significant environmental and economic risks, motivating the need for timely and reliable surface leak detection techniques. This paper presents a proof-of-concept study that investigates the use of UAV-based multispectral imagery and deep learning for detecting and distinguishing surface oil and water leaks over soil backgrounds. Multispectral data were acquired using a UAV-mounted sensor under controlled experimental conditions and processed through a radiometric and geometric correction pipeline. Spectral analysis was conducted to assess band-wise separability, highlighting the effectiveness of Red and Red-Edge bands for oil–water discrimination. Multiple object detection models, including YOLOv11, RT-DETR, Faster R-CNN, and a fusion-based YOLOv11-RGBT variant, were evaluated using these inputs. Experimental results demonstrate that single-band models achieve robust detection performance, with YOLOv11 attaining detection accuracies of 92.8% for oil and 98.1% for water, while RT-DETR and Faster R-CNN demonstrated comparable accuracy. The fusion-based YOLOv11-RGBT model achieved lower performance, likely due to limited dataset size for effective cross-band feature learning. Overall, the findings demonstrate that UAV-based multispectral sensing combined with deep learning offers a practical solution for localized surface leakage monitoring.**

***Index Terms*—UAV Remote Sensing, Multispectral Imaging, Surface Oil and Water Leak Discrimination, Object Detection, Deep Learning, Spectral Analysis, Environmental Monitoring**

I. INTRODUCTION

Pipeline leakage in oil and water distribution systems represents a critical challenge for modern infrastructure. This leakage typically stems from aging assets, corrosion, ground movement, inadequate monitoring, and vandalism [1]. Oil leaks can cause severe environmental damage by degrading vegetation, contaminating soil and water resources, and threatening human and aquatic health [2]. Water leakage, on the other hand, results in substantial global losses, estimated at 10–40 %, and increases operational costs due to the additional energy required for treatment and distribution [3].

Traditionally, pipeline leaks are identified through visual inspections, where surface cues such as darkened soil or abnormal vegetation indicate possible leakage. Beyond direct observation, ground-based methods like acoustic sensing and ground-penetrating radar offer effective alternatives by leveraging indirect measurements [4–7], but these methods are often expensive, labor-intensive, and limited in coverage. Inline inspection robots equipped with cameras and sensors can detect internal defects such as cracks and corrosion in real time [8, 9]; however, their use is confined to localized inspections and unsuited for wide-area monitoring.

Remote sensing provides a non-invasive and scalable solution for large-scale leakage monitoring. Various sensors can be integrated into satellite and UAV platforms, ranging from passive systems such as multispectral, thermal, hyperspectral, and infrared imaging to active technologies like LiDAR, radar, and laser fluorosensors [10]. Satellite based studies have demonstrated strong potential for oil and water detection; for example, [11] evaluated extensive band and band-ratio combinations to achieve near-perfect oil–water separability for marine oil spill detection, while [12] employed a convolutional neural network to classify satellite images into leak and non-leak categories, with 81% accuracy. While satellite missions like Sentinel, Landsat, and RADARSAT provide extensive coverage, UAV platforms with their low-alitude operation delivers higher spatial resolution and flexibility, capturing localized or early-stage leaks that satellite imagery often misses. Specifically, [13] evaluated three UAV-mounted sensors for underground water pipeline leak detection, where ground-penetrating radar outperformed thermal and multispectral cameras across various burial depths. Using UAV-mounted multispectral sensors, [14] detected oil pollution on water surfaces through spectral brightness indices, while [15] introduced ResS-UNet, a lightweight semantic segmentation framework for terrestrial oil spill detection that achieves a recognition accuracy of 96.52% even with small multispectral datasets. Despite these advances, most existing studies address oil [16, 17] or water [18, 19] leakage independently, or focus on oil-on-water scenarios [20, 21], with limited work on distinguishing oil and water leaks over soil backgrounds. This distinction is important because both leak types can appear visually similar under RGB imaging, yet require different mitigation responses. Motivated by this gap, this study proposes a UAV-based multispectral imaging framework for detecting and distinguishing oil and water surface leaks over soil using deep learning. This study evaluates passive sensing under controlled field conditions, identifies informative spectral bands, and evaluates various deep learning architectures. The paper is organized as follows: Section II presents data acquisition, spectral analysis, and model evaluation; Section III reports results; and Section IV discusses findings, limitations, and implications.

II. Methodology

A. UAV-Based Multispectral Data Acquisition and Processing

Multispectral data were acquired using a MicaSense RedEdge-P camera rigidly mounted on the lower frame plate of a standard quadcopter (UAV) to ensure stable alignment and minimal vibration. The camera was enclosed in a housing powered by an independent battery. The UAV was also equipped with a Pixhawk Orange Cube flight controller, a Here3+ GNSS module, and a 6-cell 10,000 mAh Li-Po battery, resulting in a 3 kg takeoff weight with a 30-minute flight duration. The RedEdge-P camera captures five multispectral bands (Blue, Green, Red, Red-Edge, and Near-Infrared (NIR)) each with a resolution of 1456 $\times$ 1088 pixels (1.6 MP), along with a high-resolution panchromatic band of 2464 $\times$ 2056 pixels[22]. All imagery was stored onboard for offline processing.

Data were acquired over multiple UAV flights across three days at 15–25 m AGL and 2 m/s under clear-sky conditions (10:00 AM–1:00 PM), with most spill events imaged within 30 minutes. Experiments used multiple 1 m $\times$ 1 m soil patches (dark gardening soil mixed with red soil), spaced 10 m apart, with oil volumes of 5–50 ml and water volumes of 100–400 ml. Selected plots included up to 60% vegetation. Flights were pre-planned using Mission Planner with 80% forward overlap and 60% sidelap, yielding a ground sampling distance of 0.94–1.57 cm/pixel. Additional dataset details and results are available at: https://surface-leakage-detection.github.io/

Prior to each flight, radiometric calibration was performed using a calibrated reflectance panel to derive band-specific coefficients and apply dark-frame corrections [23]. The multispectral images were subsequently processed through an offline pipeline comprising radiometric correction, geometric band co-registration, and pan-sharpening. The co-registration step utilizes precomputed warp matrices to align all spectral bands into a spatially consistent stack, ensuring each pixel represents the same geographic point. This process generates spatially enhanced outputs, including radiometrically corrected multispectral data and metadata essential for reproducible analysis [24, 25]. An overview of the UAV-based data acquisition and processing workflow is shown in Fig. 1.

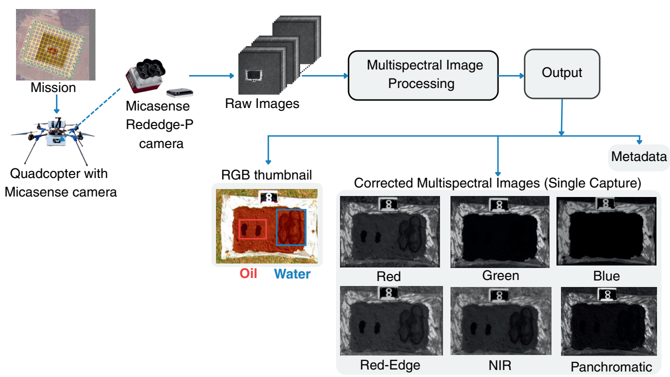

Fig. 1. Overview of the UAV-based multispectral data acquisition and processing pipeline

B. Spectral Analysis for Band Selection

A systematic, band-wise analysis was performed on radiometrically corrected multispectral data to identify the most informative spectral bands for oil–water discrimination on soil surfaces, utilizing the following methods:

1) Histogram-Based Spectral Response Analysis: Histogram analysis was performed to assess oil–water separability by comparing pixel intensity distributions across individual spectral bands. As shown in Fig. 2, the Red-Edge band exhibits the strongest separation between oil and water, with clearly separated peaks and minimal overlap. The Red band also shows discernible separation, though with greater overlap between classes. In contrast, the Blue, NIR, and Panchromatic bands display substantial overlap, indicating limited discriminative capability under the tested conditions.

2) Statistical Separability Analysis: To complement the histogram analysis, first-order statistical measures, including class-wise mean and variability, were computed for each band to assess inter-class separability and intra-class variability. Additionally, the Jeffries–Matusita (JM) [26] distance was used as a probabilistic separability metric, as it captures differences between full class distributions rather than relying solely on mean separation. Higher mean differences, lower variance, and larger JM values indicate improved discriminative potential. Table I summarizes the statistical separability results.

TABLE I
Spectral Statistics and Jeffries–Matusita (JM) Separability for Oil and Water

Band	**Mean$_W$**	**Mean$_O$**	**Δ**	**JM**
Red (668 nm)	15 212.47	12 614.65	$\sim$2 598	0.2918
Green (560 nm)	14 079.61	11 044.08	$\sim$3 035	0.4964
Blue (475 nm)	7 328.22	8 175.25	$\sim$847	0.1642
Red-Edge (717 nm)	20 766.75	15 916.18	$\sim$4 850	0.6545
NIR (842 nm)	22 269.29	22 262.17	$\sim$7	0.0335
Panchromatic (634.5 nm)	15 400.45	15 709.60	$\sim$309	0.0821

The Red-Edge band achieves the highest inter-class mean difference ($\Delta \approx 4850$ DN) and the largest JM distance among individual bands, indicating superior oil–water separability due to lower intra-class variability. Although the Red band shows substantial mean separation ($\Delta \approx 2598$ DN); but increased intra-class variability reduces its JM value. Conversely, the Blue, NIR, and Panchromatic bands exhibit minimal mean differences and near-zero JM distances, confirming their limited suitability for oil–water discrimination.

To evaluate the combined contribution of the Red and Red-Edge bands, a multivariate JM distance was computed. The result (JM = 0.673) indicates moderate improvement, suggesting that multi-band information can enhance oil–water discrimination, particularly where individual band responses are ambiguous. As shown in Table I, the Green band exhibits moderate separability (JM = 0.4964) due to high intra-class variability. Despite slight JM improvements (0.668) when paired with Red-Edge, the Green band was excluded in favor of Red and Red-Edge due to poor visual contrast (Fig. 1) and weak preliminary detection results.

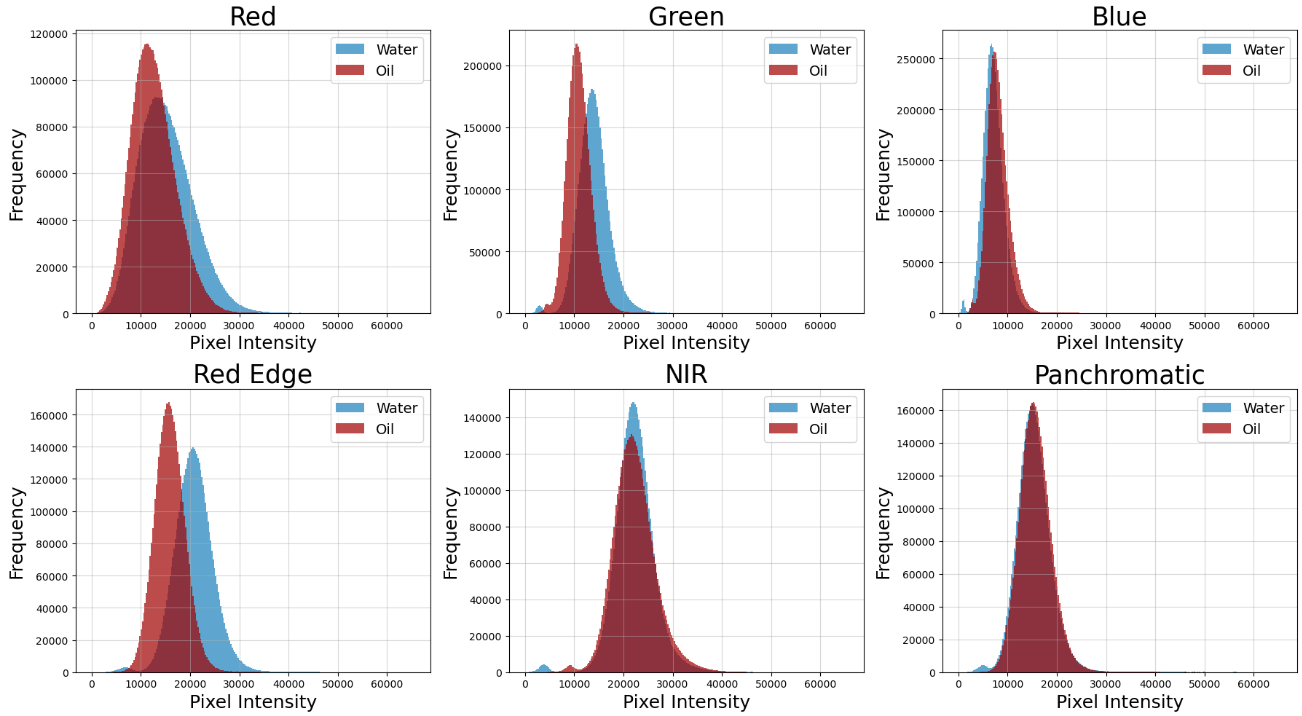

Fig. 2. Histogram comparison of oil and water pixel intensity distributions across spectral bands, with the Red-Edge band exhibiting the highest separability.

C. Multispectral Dataset Preparation and Comparative Model Evaluation

Based on spectral analysis, a dataset of 512 Red and Red-Edge images was constructed. Single-channel 16-bit `.tif` images acquired from the multispectral sensor were converted to three-channel 8-bit RGB format for compatibility with standard object detection frameworks, with intensities normalized to 0–255 using `Pillow (PIL)` [27] and `Rasterio` [28]. Images were manually annotated in `LabelImg` [29] with two classes: *oil* and *water*, and divided using a standard 80:20 training/validation split widely adopted in detection literature. To compare complementary detection paradigms, YOLOv11 [30], RT-DETR [31], and Faster R-CNN [32] were selected, representing one-stage, transformer-based, and two-stage detectors, respectively. YOLOv11 emphasizes real-time efficiency, RT-DETR uses global attention for feature reasoning, while Faster R-CNN provides a strong localization baseline. These detectors were trained independently on Red and Red-Edge inputs. In addition, YOLOv11-RGBT [33], a mid-fusion multispectral detection framework, was evaluated to examine whether combining both bands improves performance. All experiments were implemented in PyTorch 2.5.1 with CUDA 12.1 and cuDNN 8.9.7. System specifications are summarized in Table II.

TABLE II
SYSTEM SPECIFICATIONS FOR MODEL TRAINING AND EVALUATION

Component	Training	Evaluation
Operating System	Windows 11 Pro	Ubuntu 22.04.5 LTS
CPU	AMD Ryzen 9 7950X3D	Intel i7-12700K (12th Gen)
GPU	RTX A6000 (48 GB)	RTX 3080 Ti (12 GB)
RAM	128 GB DDR5	16 GB DDR4

III. EXPERIMENTAL RESULTS

A. Oil and Water Leak Detection Performance

Each model was trained on the proposed multispectral dataset using pretrained COCO weights, with performance metrics summarized in Table III. Among the architectures, YOLOv11 and RT-DETR achieved superior performance, both exceeding 0.98 mAP@50 overall. YOLOv11 provided the highest localization precision (0.806 mAP@50:95), while RT-DETR demonstrated the most balanced metrics, particularly for the oil class (0.989 recall). Faster R-CNN yielded reliable detection (0.963 mAP@50) but showed significantly lower localization accuracy (0.560 mAP@50:95), indicating a performance gap in precise bounding box regression.
The fusion-based YOLOv11-RGBT model, which combines Red and Red-Edge inputs, underperformed relative to single-band models, achieving an overall mAP@50 of 0.819. The reduced performance, particularly the lower oil recall (0.665), suggests that standard mid-level fusion architectures may require larger datasets to learn effective cross-modal representations.

B. Computational Performance and Inference Efficiency

Per-image processing time was evaluated for each model on the evaluation system listed in Table II. The reported times include multispectral processing, image saving, and inference, while the one-time warp matrix generation time is excluded. As summarized in Table IV, YOLOv11 achieved the lowest inference time (0.016 s), demonstrating suitability for near real-time operation, whereas the fusion-based YOLOv11-RGBT incurred higher latency due to dual-channel feature fusion.

TABLE III
PERFORMANCE METRICS OF MODELS ON OIL AND WATER DETECTION

Model	Class	mAP@50	mAP@50:95	Precision	Recall	Red	Red-Edge
YOLOv11	Oil	0.984	0.714	0.960	0.914	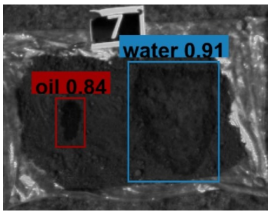	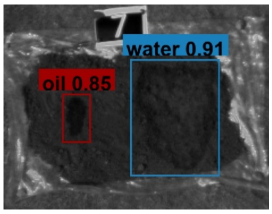
	Water	0.994	0.899	0.983	0.987		
	Overall	0.989	0.806	0.972	0.951		
Faster R-CNN	Oil	0.933	0.427	0.933	0.957	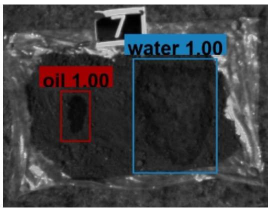	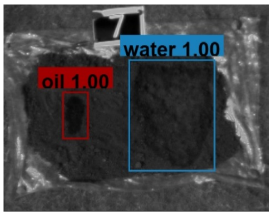
	Water	0.993	0.693	0.993	1.000		
	Overall	0.963	0.560	0.963	0.979		
RT-DETR	Oil	0.991	0.719	0.978	0.989	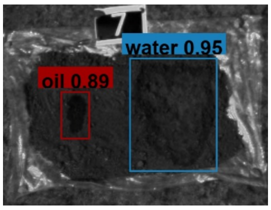	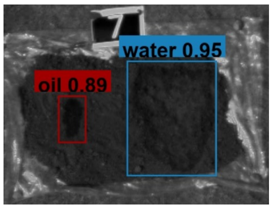
	Water	0.994	0.877	0.988	0.992		
	Overall	0.992	0.798	0.983	0.990		
YOLOv11-RGBT	Oil	0.751	0.397	0.821	0.665	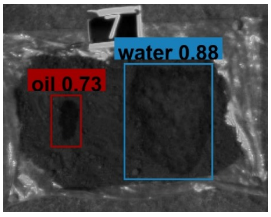	
	Water	0.887	0.663	0.934	0.827		
	Overall	0.819	0.512	0.832	0.737		

Resources: The multispectral dataset, performance metrics (loss plots, mAP curves, and confusion matrices), and extended analysis of additional test and unseen images are publicly available at the project website: https://surface-leakage-detection.github.io/

TABLE IV
MODEL PROCESSING TIME FOR A SINGLE IMAGE

Metric	YOLOv11	Faster R-CNN	RT-DETR	YOLOv11-RGBT (fusion)
Warp Matrix Gen.†	38.0 s (one-time per flight, excluded)			
Multispectral Proc. & Save	72.73 µs			
Inference Time (s)	**0.016**	**0.042**	**0.027**	**0.109**
Total Time (s)	0.01607	0.04207	0.02707	0.10907

† The warp matrix is generated once per flight by fusing a set of panel and multispectral images, hence its exclusion from per-image analysis.

IV. DISCUSSION

Experimental results demonstrate that UAV-based multispectral imagery can reliably distinguish surface oil and water leaks over soil backgrounds, with spectral analysis identifying the Red and Red-Edge bands as the most discriminative. Using these bands, YOLOv11 and RT-DETR achieved high detection accuracy, successfully identifying oil leak volumes as low as 5 ml and maintaining robustness under partial occlusion and vegetation-induced shadowing. A key outcome of this study is the real-time feasibility of the proposed pipeline. As shown in Table IV, the YOLOv11 inference time of approximately 0.01 s accounts for less than 5% of the 0.33 s six-band acquisition interval, confirming that a suitable companion computer can perform onboard detection without data bottlenecks.

Despite high accuracy at low volumes, generalizing models for operational use remains challenging due to limited data and single-site acquisition. Future efforts will focus on expanding the dataset to include varied illumination, surface heterogeneity, and altitudes up to 100 m AGL. This dataset will facilitate a transition from pre-trained weights to training from scratch. Future work will also investigate six-band fusion, driven by the full stack's high 1.284 JM distance. In parallel, custom spectral indices will be evaluated, as these approaches may improve oil–water separability beyond the single and dual-band methods evaluated in this study. Through these advancements, we aim to bridge the gap between experimental validation and deployment of fully autonomous, real-time surface leak detection systems for critical energy infrastructure.

ACKNOWLEDGMENT

This research was funded by the Centre of Excellence in Oil, Gas and Energy (CoE-OGE), IIT Bombay. The authors sincerely thank the collaborating PSUs namely IOCL, GAIL, and HPCL, and Dr. Kannan Chandrasekaran (CoE-OGE Chair Professor) for technical guidance, and acknowledge Mr. Omar Kashmar, whose thesis was used for preliminary evaluations of multispectral and thermal imaging systems.

References

[1] CONCAWE, "Performance of european cross-country oil pipelines: Statistical summary of reported spillages in 2013 and since 1971," CONservation of Clean Air and Water in Europe, Brussels, Belgium, Tech. Rep. Report No. 4/15, 2015, accessed: Jul. 28, 2015. [Online]. Available: https://www.concawe.eu/uploads/Modules/Publications/rpt_15-4.pdf

[2] H. Umar, M. A. Khanan, C. Ogbonnaya, M. Shiru, A. Ahmad, and A. Baba, "Environmental and socioeconomic impacts of pipeline transport interdiction in niger delta, nigeria," *Heliyon*, vol. 7, no. 5, 2021.

[3] B. Shakmak and A. Al-Habaibeh, "Detection of water leakage in buried pipes using infrared technology; a comparative study of using high and low resolution infrared cameras for evaluating distant remote detection," in *2015 IEEE Jordan Conference on Applied Electrical Engineering and Computing Technologies (AEECT)*. IEEE, 2015, pp. 1–7.

[4] H. V. Fuchs and R. Riehle, "Ten years of experience with leak detection by acoustic signal analysis," *Applied acoustics*, vol. 33, no. 1, pp. 1–19, 1991.

[5] T. Tucciarelli, A. Criminisi, and D. Termini, "Leak analysis in pipeline systems by means of optimal valve regulation," *Journal of Hydraulic Engineering*, vol. 125, no. 3, pp. 277–285, 1999.

[6] F. Paquin, D. Babineau, F. Brissette, and R. Leconte, "Développement d'une méthodologie de repérage des conduites d'aqueduc présentant des fuites," *Canadian Journal of Civil Engineering*, vol. 27, no. 1, pp. 151–159, 2000.

[7] O. B. Zainon, N. A. N. Zahairy, and M. D. Ghazali, "Detecting water leakage patterns using ground penetrating radar in clay and sandy soils," *Journal of Advanced Geospatial Science & Technology*, vol. 4, no. 2, pp. 187–204, 2024.

[8] J. M. M. Tur and W. Garthwaite, "Robotic devices for water main in-pipe inspection: A survey," *Journal of Field Robotics*, vol. 27, no. 4, pp. 491–508, 2010.

[9] L. Yu, E. Yang, P. Ren, C. Luo, G. Dobie, D. Gu, and X. Yan, "Inspection robots in oil and gas industry: a review of current solutions and future trends," in *2019 25th International Conference on Automation and Computing (ICAC)*. IEEE, 2019, pp. 1–6.

[10] C. Gómez and D. R. Green, "Small unmanned airborne systems to support oil and gas pipeline monitoring and mapping," *Arabian Journal of Geosciences*, vol. 10, no. 9, p. 202, 2017.

[11] M. Zakzouk, I. Abou El-Magd, E. M. Ali, A. M. Abdulaziz, A. Rehman, and T. Saba, "Novel oil spill indices for sentinel-2 imagery: A case study of natural seepage in qaruh island, kuwait," *MethodsX*, vol. 12, p. 102520, 2024.

[12] E. Fajardo and D. Moctezuma, "Water leak detection through satellite imagery and deep learning," *Sustainable Water Resources Management*, vol. 11, no. 2, p. 33, 2025.

[13] D. Voysey and G. Campbell, "Assessing the detectability of underground water-pipe leaks with non-invasive technologies," in *Proc. Assoc. Public Auth. Surv. Conf*, vol. 26, 2023, pp. 79–86.

[14] K. A. Vytovtov, E. A. Barabanova, T. Y. Gladkikh, A. L. Kulina, and G. K. Vytovtov, "Remote monitoring of water pollution with oil products in the visible range by using uav multispectral camera," in *2022 International Conference on Information, Control, and Communication Technologies (ICCT)*. IEEE, 2022, pp. 1–5.

[15] J. Xing, Y. Zhang, B. Li, Z. Cao, C. Zhan, Y. Liu, M. Hao, and Z. Jiang, "Terrestrial oil spills recognition based on small samples from uav multispectral images," *IEEE Sensors Journal*, 2024.

[16] M. Mahdianpari, B. Salehi, F. Mohammadimanesh, G. Larsen, and D. R. Peddle, "Mapping land-based oil spills using high spatial resolution unmanned aerial vehicle imagery and electromagnetic induction survey data," *Journal of applied remote sensing*, vol. 12, no. 3, pp. 036 015–036 015, 2018.

[17] J. R. Dean, S. Ahmed, W. Cheung, I. Salaudeen, M. Reynolds, S. L. Bowerbank, C. E. Nicholson, and J. J. Perry, "Use of remote sensing to assess vegetative stress as a proxy for soil contamination," *Environmental Science: Processes & Impacts*, vol. 26, no. 1, pp. 161–176, 2024.

[18] S. Traore, G. Fipps, C. Swanson, J. Dufek, and M. Robin, "Unmanned aerial vehicle system integrating high-resolution sensors for detecting leaks in irrigation canals—proof of concept," *Irrigation and Drainage*, vol. 71, no. 1, pp. 206–217, 2022.

[19] C. Chatelard, J. S. Muñoz, J.-C. Krapez, C. Mazel, V. Olichon, J. B. Polo, Y.-M. Frédéric, F. Hélias, P. Barillot, I. Legoff *et al.*, "Leak detection in water transmission systems by multispectral remote sensing with airplane and uav," in *IGARSS 2019-2019 IEEE International Geoscience and Remote Sensing Symposium*. IEEE, 2019, pp. 7124–7127.

[20] T. Y. Gladkikh, K. D. Rusakov, and A. V. Grafenkov, "Oil pollution detection in aquatic ecosystems using uavs and multispectral imaging based on deep learning technologies," in *2024 8th International Conference on Information, Control, and Communication Technologies (ICCT)*. IEEE, 2024, pp. 1–5.

[21] N. A. Bui, Y. Oh, and I. Lee, "Oil spill detection and classification through deep learning and tailored data augmentation," *International Journal of Applied Earth Observation and Geoinformation*, vol. 129, p. 103845, 2024.

[22] AgEagle Aerial Systems Inc., "Micasense rededge-p: Multispectral and panchromatic imaging system," Product Brochure, 2022, online. [Online]. Available: https://ageagle.com/wp-content/uploads/2022/08/AgEag

le-RedEdge-P-Brochure-EN.pdf
[23] MicaSense Support, "How to use the calibrated reflectance panel (CRP)," https://support.micasense.com/hc/en-us/articles/1500001975662-How-to-use-the-Calibrated-Reflectance-Panel-CRP, 2024, accessed: January 7, 2026.
[24] MicaSense Radiometric, "Radiometric calibration model for MicaSense sensors," https://support.micasense.com/hc/en-us/articles/115000351194-Radiometric-Calibration-Model-for-MicaSense-Sensors, 2024, accessed: January 7, 2026.
[25] MicaSense, "MicaSense image processing library," https://github.com/micasense/imageprocessing, 2024, accessed: January 7, 2026.
[26] P. Swain and R. King, "Two effective feature selection criteria for multispectral remote sensing," *LARS technical reports*, p. 39, 1973.
[27] A. Clark *et al.*, "Pillow (pil fork) — python imaging library," Python Software Foundation, 2024, version 10.4.0. [Online]. Available: https://python-pillow.org
[28] S. Gillies *et al.*, "Rasterio: Access to geospatial raster data," Python Software Foundation, 2024, version 1.4.3. [Online]. Available: https://github.com/rasterio/rasterio
[29] Tzutalin, "Labelimg: Image labeling tool," GitHub Repository, 2015, online. [Online]. Available: https://github.com/tzutalin/labelImg
[30] R. Khanam and M. Hussain, "Yolov11: An overview of the key architectural enhancements," *arXiv preprint arXiv:2410.17725*, 2024.
[31] Y. Zhao, W. Lv, S. Xu, J. Wei, G. Wang, Q. Dang, Y. Liu, and J. Chen, "Detrs beat yolos on real-time object detection," in *Proceedings of the IEEE/CVF conference on computer vision and pattern recognition*, 2024, pp. 16 965–16 974.
[32] S. Ren, K. He, R. Girshick, and J. Sun, "Faster r-cnn: Towards real-time object detection with region proposal networks," *IEEE transactions on pattern analysis and machine intelligence*, vol. 39, no. 6, pp. 1137–1149, 2016.
[33] D. Wan, R. Lu, Y. Fang, X. Lang, S. Shu, J. Chen, S. Shen, T. Xu, and Z. Ye, "Yolov11-rgbt: Towards a comprehensive single-stage multispectral object detection framework," *arXiv preprint arXiv:2506.14696*, 2025.